

Exceptional points of any order in a generalized Hatano-Nelson model

Julius T. Gohsrich,^{1,2,*} Jacob Fauman,^{1,2} and Flore K. Kunst^{1,†}

¹Max Planck Institute for the Science of Light, Staudtstraße 2, 91058 Erlangen, Germany

²Department of Physics, Friedrich-Alexander Universität Erlangen-Nürnberg, Staudtstraße 7, 91058 Erlangen, Germany

(Dated: March 19, 2024)

Exceptional points (EPs) are truly non-Hermitian (NH) degeneracies where matrices become defective. The order of such an EP is given by the number of coalescing eigenvectors. On the one hand, most work focusses on studying N th-order EPs in $N \leq 4$ -dimensional NH Bloch Hamiltonians. On the other hand, some works have remarked on the existence of EPs of orders scaling with system size in models exhibiting the NH skin effect. In this letter, we introduce a new type of EP and provide a recipe on how to realize EPs of arbitrary order not scaling with system size. We introduce a generalized version of the paradigmatic Hatano-Nelson model with longer-range hoppings. The EPs existing in this system show remarkable physical features: Their associated eigenstates are localized on a subset of sites and are exhibiting the NH skin effect. Furthermore, the EPs are robust against generic perturbations in the hopping strengths as well as against a specific form of on-site disorder.

Non-Hermitian (NH) operators, while violating the axioms of quantum mechanics, have many applications in classical setups, such as electric circuits [1, 2] and optical metamaterials [3], while also being highly relevant for open quantum systems [4] and closed strongly correlated systems [5, 6]. In recent years, non-Hermiticity has been studied from the perspective of topology, revealing rich, novel phenomena and resulting in an exciting cross-disciplinary research field [7, 8].

While the conventional bulk-boundary correspondence (BBC) is generally broken in NH models and needs to be modified [9–11], an additional, truly NH BBC correspondence can be established, which directly relates the spectral topology under periodic boundary conditions (PBCs) captured by a spectral winding number [12] to the piling of bulk states on the boundaries under open boundary conditions (OBCs) [13, 14], known as the NH skin effect (NHSE) [11]. This NHSE is always accompanied by the appearance of exceptional points (EPs) with an order scaling with system size [7, 15]. EPs are truly NH degeneracies, at which the NH Hamiltonian is defective and whose order is set by the number of coalescing eigenvectors [16]. Indeed, it is straightforward to see how such an EP emerges in a system with skin states by considering the paradigmatic Hatano-Nelson (HN) model [17, 18].

In this nearest-neighbor hopping model with asymmetric hopping strengths all states pile up on the boundary as dictated by the dominant hopping parameter. In the extreme limit where one hopping is set to zero, all states coalesce onto one at the boundary thus forming an EP with an order scaling with the number of sites.

EPs are ubiquitous [19], and naturally appear in any NH system. In particular, it has been shown that symmetries can aid to find EPs of higher-order in lower-dimensional systems [20–25]. In fact, it was recently pointed out that the much weaker condition of having a similarity has the same consequences [26]. All these studies mainly focus on the appearance of EPs of the order of the system size N . While a few remarks are made about the appearance of EP ms with $m < N$ in Refs. 23–25, and EP3s and EP4s are found in an SSH chain under OBC in Ref. 27, there is not yet a systematic study of how to generate EPs of any order m in an N -dimensional system. In this letter, we propose a method for finding such lower-order EPs by studying models akin to the HN model.

In particular, we study a family of generalized HN models, which only allow hoppings l sites to the left and r sites to the right as sketched in Fig. 1. The generalized HN model and similar models have mainly been studied in the thermodynamic limit in the mathematics [28, 29] and physics literature [30–33], especially in the context of the generalized Brillouin zone theory [11, 34, 35]. Here, we focus on features of these models for *finite* system sizes, and reveal a generic mechanism in which EP ms appear. Interestingly, while the appearance of such EPs depends on the system size N , its order does not scale with it. This behavior finds its root in a generalized chiral symmetry [36], which imposes a rotational symmetry in the spectrum shown in Fig. 2, pinning the EPs to the center of rotation.

We find that all eigenstates exhibit the NHSE, including the ones associated with the EPs, which are localized

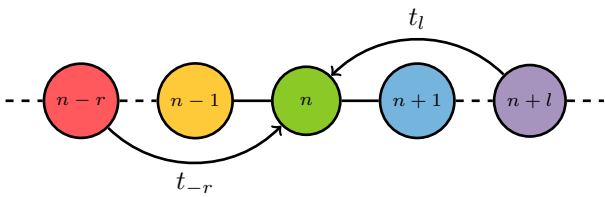


Figure 1. The generalized HN model with hoppings t_l (t_{-r}) hopping l (r) sites to the left (right). Each site contains its site index, and the model is $(l+r)$ -partite. It reduces to the customary HN model for $l = r = 1$.

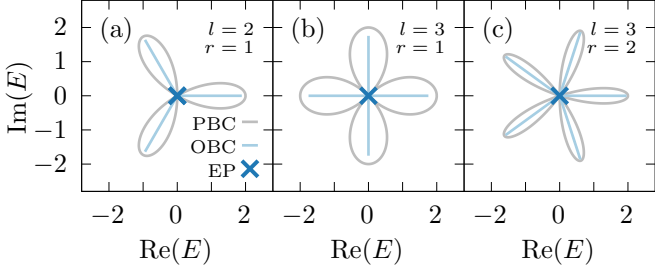


Figure 2. PBC (gray) and OBC (light blue) spectra of the generalized HN model with $t_l = t_{-r} = 1$ and l and r as indicated in the thermodynamic limit. Due to the $(l+r)$ -fold spectral rotational symmetry we find for appropriate system size an EP2, EP3, and EP4, in (a), (b), and (c), respectively, marked with a blue cross.

on a specific set of sites. Indeed, the system is $(l+r)$ -partite so that we can subdivide the system into sublattices (SLs). Furthermore, we show that it is possible to localize the EP and the remaining eigenstates on opposite ends of the chain. Lastly, we realize that the EPs are robust against generic perturbations in the hopping strengths [37, 38], and are thus protected by the spatial topology of the model. The EPs are also robust against a particular type of on-site disorder, which only exists on certain SLs. In the following, we discuss all of these features in detail.

Generalized Hatano-Nelson model.—The family of generalized HN models we investigate, cf. Fig. 1, is described by

$$H_{lr} = \sum_{n=1}^N (t_l c_n^\dagger c_{n+l} + t_{-r} c_n^\dagger c_{n-r}), \quad (1)$$

where the chain has N sites, c_n (c_n^\dagger) annihilates (creates) an excitation on site n , the first (second) term describes the hopping of l (r) sites to the left (right) with hopping strength t_l (t_{-r}), and we consider OBCs throughout this letter unless stated otherwise. Without loss of generality, we set $t_l, t_{-r} > 0$ and require $l \geq r \geq 1$ coprime, so that l and r have a greatest common divisor of one, i.e., $\gcd(l, r) = 1$, which we justify below. We note that whereas the HN model is NH iff $t_1 \neq t_{-1}$, the generalized HN model is always NH even when $t_l = t_{-r}$ as long as $l \neq r$. Let us focus on a paradigmatic example in the following before we return to the general case.

Example: $l = 2$ and $r = 1$.—We consider H_{21} shown in Fig. 3(a) with the characteristic polynomial given by

$$\chi(E) = (-E)^d \sum_{m=0}^q \binom{N-2m}{m} (t_2 t_{-1})^m (-E^3)^{q-m},$$

where $N = 3q + d$ with $0 \leq d < 3$, i.e., $q = \lfloor N/3 \rfloor$ is the quotient and $d = N \bmod 3$ is the remainder of the Euclidean division, see Appendix A. The spectrum of H_{21} is given by $\{E : \chi(E) = 0\}$, from which one

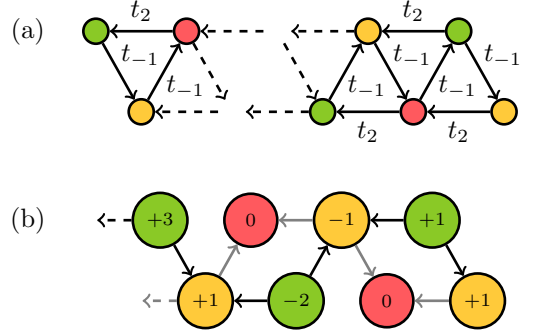


Figure 3. Generalized HN model for $l = 2$ and $r = 1$ under OBCs. (a) Alternative representation of Fig. 1 revealing the 3 SLs in red (SL_1), yellow (SL_2) and green (SL_3). (b) Visualization of the zero-energy eigenvector $|v_1\rangle$ (generalized eigenvector $|v_2\rangle$) for $t_2 = t_{-1} = 1$ on the yellow (green) SL with weights inside each node, forming the Jordan chain associated with the EP2 when the system size satisfies $N \equiv -1 \pmod{3}$. Acting with H_{21} on $|v_1\rangle$ ($|v_2\rangle$) annihilates on SL_1 (creates $|v_1\rangle$ on SL_2) following the gray (black) arrows.

can immediately read off spectral properties. While the factor $(-E)^d$ shows a d -fold degeneracy at zero energy, the $(-E)^3$ dependence dictates that the remaining eigenvalues come in triplets $\{E, E\omega_3, E\omega_3^2\}$ with $\omega_3 = e^{2\pi i/3}$. Thus, the complex spectrum of H_{21} exhibits a 3-fold rotational symmetry as shown in Fig. 2(a). In anticipation of the general case, we remark that the system is 3-partite. This implies we can define three SLs, SL_1 , SL_2 and SL_3 , shown in red, yellow and green in Fig. 3(a), where the site index n satisfies $n \bmod 3 = 0, 2$ and 1 , respectively.

Looking at the eigenspace structure of the d -fold degenerate zero-energy solutions, we uncover the following mechanism: For $d = 0$, there is no associated eigenspace, for $d = 1$ a single eigenvector exists, and for $d = 2$ one can readily construct a Jordan chain of length 2, i.e., there is an eigenvector $|v_1\rangle$ and a generalized eigenvector $|v_2\rangle$ satisfying $H_{21}|v_2\rangle = |v_1\rangle$, showing that the system exhibits an EP2. These vectors are given by

$$|v_1\rangle \propto \sum_{j=0}^q (-t)^{q-j} c_{3j+2}^\dagger |0\rangle, \quad (2a)$$

$$|v_2\rangle \propto (t_{-1})^{-1} \sum_{j=0}^q (q-j+1)(-t)^{q-j} c_{3j+1}^\dagger |0\rangle, \quad (2b)$$

where $t = t_2/t_{-1}$, and are visualized in Fig. 3(b). From their form one can see that the zero-energy eigenvector $|v_1\rangle$ (generalized eigenvector $|v_2\rangle$) only has weight on the yellow (green) SL, and has no weight on the red SL. Furthermore, both $|v_1\rangle$ and $|v_2\rangle$ depend on the hopping ratio t , and are thus exponentially localized on the left (right) for $t_2 > t_{-1}$ ($< t_{-1}$) revealing a footprint reminiscent of the NHSE, which we further explore in the general case.

General case.—In order to generalize to larger l and r ,

we choose the matrix representation \mathcal{H}_{lr} of Eq. (1) as

$$\mathcal{H}_{lr} = \begin{pmatrix} 0 & h_1 & 0 & \dots & 0 \\ 0 & 0 & h_2 & \ddots & \vdots \\ \vdots & & \ddots & \ddots & 0 \\ 0 & & \ddots & h_{l+r-1} & \\ h_{l+r} & 0 & \dots & \dots & 0 \end{pmatrix}, \quad (3)$$

where the h_j with $j = 1, 2, \dots, l+r$ are rectangular matrices of size $d_j \times d_{j+1}$ with $d_{l+r+1} \equiv d_1$ describing the hopping from SL_{j+1} to SL_j . We have chosen l and r coprime so that \mathcal{H}_{lr} is $(l+r)$ -partite, otherwise the system would split into $\text{gcd}(l, r)$ decoupled subsystems, where each individual subsystem can again be treated using our formalism. For compactness, we drop the indices of \mathcal{H}_{lr} when we consider arbitrary l and r . We remark that a broad class of models with Bloch Hamiltonians of the form of Eq. (3) have been investigated in Ref. 36 in the context of flat band physics.

The next step is to infer properties of \mathcal{H}^{l+r} and map them back to \mathcal{H} . As \mathcal{H} can be interpreted as a hopping model through its adjacency graph, raising \mathcal{H} to the n th power corresponds to n steps through the adjacency graph of \mathcal{H} . From Fig. 3(a) it is clear that \mathcal{H}_{21}^3 maps all states localized on SL_j back to SL_j for all j , so \mathcal{H}_{21}^3 is block diagonal, which is a general statement for all l and r taking $l+r$ steps. To set the notation, we write $\mathcal{H}^{l+r} = \text{diag}(\mathcal{H}_1, \mathcal{H}_2, \dots, \mathcal{H}_{l+r})$ with $\mathcal{H}_j = h_j \cdot h_{j+1} \cdots h_{l+r} \cdot h_1 \cdots h_{j-1}$, where each block \mathcal{H}_j with dimension $d_j \times d_j$ describes a hopping model solely on SL_j , and without loss of generality we sort the SLs so that $d_1 \leq d_j$ for all j . The SL sizes d_j are readily determined for all system sizes N . The small SLs such as SL_1 have size $d_1 = \lfloor N/(l+r) \rfloor$, whereas the large SLs have $d_j = \lceil N/(l+r) \rceil$, where $\lceil \cdot \rceil$ is the ceiling function, such that $d_j = d_1 + 1$ if $N \bmod (l+r) \neq 0$.

In Ref. 36 it was shown that one can diagonalize all the blocks \mathcal{H}_j in \mathcal{H}^{l+r} as $\mathcal{H}_j|u_s^j\rangle = E_s|u_s^j\rangle$, $s = 1, 2, \dots, d_1$, where the E_s are the same for all j . For all larger SLs with $d_j > d_1$, all remaining energies are zero, i.e., $\mathcal{H}_j|u_t^j\rangle = 0$, $t = d_1 + 1, \dots, d_j$. In our case we have at most one zero-energy solution per SL and we relabel their corresponding eigenvectors as $|u_0^j\rangle$. Having the full spectrum of \mathcal{H}^{l+r} , the spectrum of \mathcal{H} consists of $d = \sum_{j=2}^{l+r} (d_j - d_1)$ zero energies, which is in our case the number of large SLs, i.e., $d = N \bmod (l+r)$, and the $(N - d)$ energies $\{\sqrt[N]{E_s}, \omega_n \sqrt[N]{E_s}, \dots, \omega_n^{n-1} \sqrt[N]{E_s} : s = 1, \dots, d_1\}$, where $\omega_n = e^{2\pi i/n}$ with $\omega_n^n = 1$ and $n = l+r$. This was shown in Ref. 36 by leveraging that Eq. (3) obeys a generalized chiral symmetry $\mathcal{C}_n : \Gamma_n \mathcal{H} \Gamma_n^{-1} = \omega_n^{-1} \mathcal{H}$, where the generalized chiral operator is $\Gamma_n = \text{diag}(\mathbb{1}_{d_1}, \omega_n \mathbb{1}_{d_2}, \dots, \omega_n^{n-1} \mathbb{1}_{d_n})$, with $\mathbb{1}_m$ the m -dimensional identity matrix, satisfying $\Gamma_n \Gamma_n^{-1} = \Gamma_n^n = \mathbb{1}_N$. In our previous example, we saw all these implications from the characteristic polynomial.

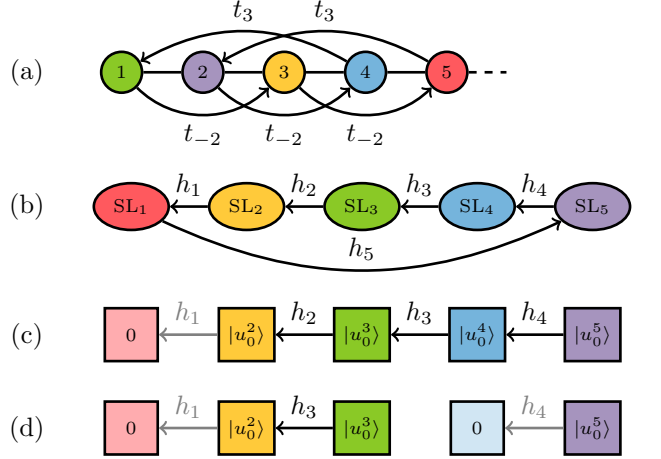


Figure 4. Determination of the EP structure of the generalized HN model with $l = 3$ and $r = 2$. (a) shows the hopping model in the site basis with corresponding site index inside each node and SL coloring corresponding to (b). Increasing N one by one, the sizes of $\text{SL}_3, \text{SL}_5, \text{SL}_2, \text{SL}_4, \text{SL}_1$ are increased cyclically. Starting with $N \equiv 4 \bmod 5$ in (c), the generalized zero-energy eigenvectors form a Jordan chain of length 4 corresponding to an EP4. Decreasing the system size to $N \equiv 3 \bmod 5$ in (d) removes $|u_0^4\rangle$ on SL_4 and splits the Jordan chain into one of length 1, corresponding to an one-dimensional zero-energy subspace, and a Jordan chain of length 2 corresponding to an EP2. For $N \equiv 2 \bmod 5$, $N \equiv 1 \bmod 5$ and $N \equiv 0 \bmod 5$ one finds two, one and zero one-dimensional zero-energy subspaces of \mathcal{H} , respectively (not depicted).

Besides these spectral considerations we analyze the eigenvectors of \mathcal{H} . First, it is instructive to define the padded eigenvectors $|\tilde{u}_s^j\rangle$ so that they are the eigenvectors of \mathcal{H}^{l+r} . The eigenvectors $|w_s^p\rangle$ of \mathcal{H} associated with $s \neq 0$, i.e., $E_s \neq 0$ are given by

$$|w_s^p\rangle \propto \sum_{\nu=0}^{l+r-1} \left(E_s e^{2\pi i/p} \right)^{-\frac{\nu}{l+r}} \mathcal{H}^\nu |\tilde{u}_s^1\rangle, \quad (4)$$

where $p = 1, \dots, l+r$ and we set $\mathcal{H}^0 = \mathbb{1}_N$. Compared to the eigenvectors of \mathcal{H}^{l+r} , the $|w_s^p\rangle$ have weight on all SLs.

Coming to the zero-energy eigenvectors, we use that $\mathcal{H}^{l+r} |\tilde{u}_0^j\rangle = 0$, which shows that all $|\tilde{u}_0^j\rangle$ are on the one hand zero-energy eigenvectors of \mathcal{H}^{l+r} , while on the other hand they are generalized eigenvectors of \mathcal{H} by definition. However, a priori it is not clear what the length $m \leq l+r$ of the associated Jordan chain defining an EP m is. As we will show, it is enough to keep track of consecutive SLs with $d_j = d_1 + 1$ to determine m . Let us start on SL_{j-1} of size $d_{j-1} = d_1$ followed by SL_j of size $d_j = d_1 + 1$. Then we know that $|\tilde{u}_0^j\rangle$ is a proper eigenvector of \mathcal{H}^{l+r} as $\mathcal{H}^{l+r} |\tilde{u}_0^j\rangle = h_{j-1} |\tilde{u}_0^j\rangle = 0$. While SL_{j+1} up to SL_{j+m} have the same size $d_{j+1} = \dots = d_{j+m} = d_1 + 1$, the Jordan chain $h_j |\tilde{u}_0^{j+1}\rangle = |u_0^j\rangle, \dots,$

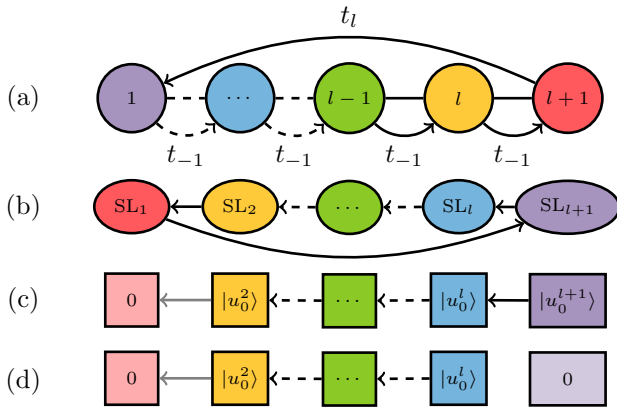


Figure 5. Determination of the EP structure of the generalized HN model for arbitrary l and $r = 1$ similar to Fig. 4. (a) Increasing the chain length increases the sizes of SLs cyclically in (b). Starting with $N \equiv -1 \pmod{l+1}$ corresponds to having an EP l in (c). Successively decreasing the size of the chain always removes the generalized eigenvector with the highest SL index as shown in (d).

$h_{j+m-1}|u_0^{j+m}\rangle = |u_0^{j+m-1}\rangle$ must continue. This comes from the fact that all h_j, \dots, h_{j+m-1} of size $d_j \times d_j$ have trivial nullspace, i.e., there exists no $|v\rangle \neq 0$ so that $h_j|v\rangle = 0$, as shown in Appendix B. Thus, if finally $d_{j+m+1} = d_1$, we identified a Jordan chain of length m and thus an EP m . Therefore, determining the lengths of all Jordan chains, i.e., the orders of all EPs, reduces to counting the number of large SLs in sequence. We remark that this procedure only depends on the existence of the zero-energy eigenvectors of the \mathcal{H}_j , and thus on $N \pmod{l+r}$ and not directly on the system size N . Fig. 4 shows how to determine the Jordan chains for $l = 3$ and $r = 2$ graphically. For completeness, we define $|w_0^p\rangle = |\tilde{u}_0^p\rangle$ so that the $|w_s^p\rangle$ are all (generalized) eigenvectors of \mathcal{H} .

General recipe towards finding EPs.—Equipped with this algorithm we show how to engineer arbitrary low-order EP ms in the generalized HN model of size N . First, for $N \equiv -1 \pmod{l+r}$ we have the $l+r-1$ generalized eigenvectors $|\tilde{u}_0^j\rangle$ with $j = 2, \dots, l+r$ forming a Jordan chain of length $l+r-1$ corresponding to an EP $(l+r-1)$ as shown in the example in Fig. 4(c). Conversely, one can design a generalized HN model exhibiting an EP m by choosing $l+r = m+1$, where $l > r \geq 1$ coprime, and system size N so that $N \equiv -1 \pmod{l+r}$.

Secondly, we can simplify this further by choosing $r = 1$. From the previous paragraph we know that the system can host up to EP l s for $N \equiv -1 \pmod{l+1}$. However, decreasing the system size one by one removes subsequently $|\tilde{u}_0^{l+1}\rangle$ down to $|\tilde{u}_0^2\rangle$, shortening the Jordan chain one by one and thus reducing the order of the EP one by one as shown in Fig. 5. Conversely, one can engineer an EP m by choosing any $l \geq m$ and $r = 1$ and choose a system size satisfying $N \equiv m \pmod{l+1}$.

The generalized HN is not restricted to featuring a single EP as one can have more elaborate zero-energy eigenspaces as already seen in the example $l = 3$ and $r = 2$ in Fig. 4(d). One can also get multiple EPs, e.g., when considering $l = 5$ and $r = 2$, one can find two EP2s for $N \equiv 4 \pmod{7}$, and an EP2 and EP3 for $N \equiv 5 \pmod{7}$.

EPs exhibiting NHSE.—Having established that the generalized HN model can host EPs of arbitrary order for an appropriate choice of l and r , we want to determine further properties of their associated eigenvectors. As extensively discussed in the literature, the NHSE is directly related to the spectral topology of NH tight-binding models, where the topological index is the spectral winding number $w(E_R) = \frac{1}{2\pi i} \int_{-\pi}^{\pi} dk \frac{d}{dk} \ln[H(k) - E_R]$, where E_R is a reference energy and the Bloch Hamiltonian $H(k)$ is in our case given by $H(k) = t_l e^{ik} + t_{-r} e^{-irk}$. The sign of the winding number predicts that the eigenstate associated with E_R is exponentially localized to the left (right) of the system when $\text{sgn } w > 0$ ($\text{sgn } w < 0$), where we note that an eigenstate is delocalized if its associated winding number is ill-defined.

We find that the correspondence is valid for all eigenvectors of the system, including the eigenvectors associated with the EPs. In the example $l = 2$ and $r = 1$, shown in Figs. 6(a,b,e,f), one can on the one hand determine the winding number at zero energy as $w(0) = 2$ (-1) if $t_2 > t_{-1}$ ($< t_{-1}$). On the other hand, the explicit form of the eigenvector $|v_1\rangle$ in Eq. (2a) only depends on powers of t_2/t_{-1} . Thus, the sign of $w(0)$ correctly predicts the occurrence and exponential localization of the NHSE associated with that state. In that example, it is interesting to notice that one can always tune t_2 and t_{-1} so that for a fixed $s \in [0, d_1]$, all eigenvectors associated with $|\sqrt[3]{E_s}| < |E_B|$ are localized on one end of the chain, while the remaining eigenvectors with $|\sqrt[3]{E_s}| > |E_B|$ are localized on the opposite end, where E_B is a Bloch point [39], i.e., a self-intersection of the PBC spectrum, separating regions of positive and negative winding numbers. One can explicitly show this by considering the real branch of the spectrum. There, the Bloch point is determined by $\text{Im}(E_B) = \text{Im}[H(k_B)] = 0$, which is solved by $k_B = 2 \arctan(\sqrt{(2t_2 - t_{-1})/(2t_2 + t_{-1})})$ if $t_{-1} < 2t_2$. In the thermodynamic limit, the maximum eigenvalue of \mathcal{H}_{21} is $E_{\max} = 3t_2^{1/3}(t_{-1}/2)^{2/3}$ [28, 32], so the largest eigenvalue for finite system sizes is lower than that. As $0 \leq E_B = t_2[(t_{-1}/t_2)^2 - 1] \leq E_{\max}$, we can always tune t_2 and t_{-1} appropriately. We can especially separate the eigenvector associated with the EP from the rest of the eigenvectors as shown in Figs. 6(b,c,f).

Robustness of the EPs and the NHSE.—Now, let us review the robustness of the EPs against perturbations. We find two types of perturbations, which leave the EPs unaltered, namely generic perturbations to the hopping strengths and arbitrary on-site disorder on specific SLs. We discuss these two types of perturbation, also with respect to the NHSE, in the following.

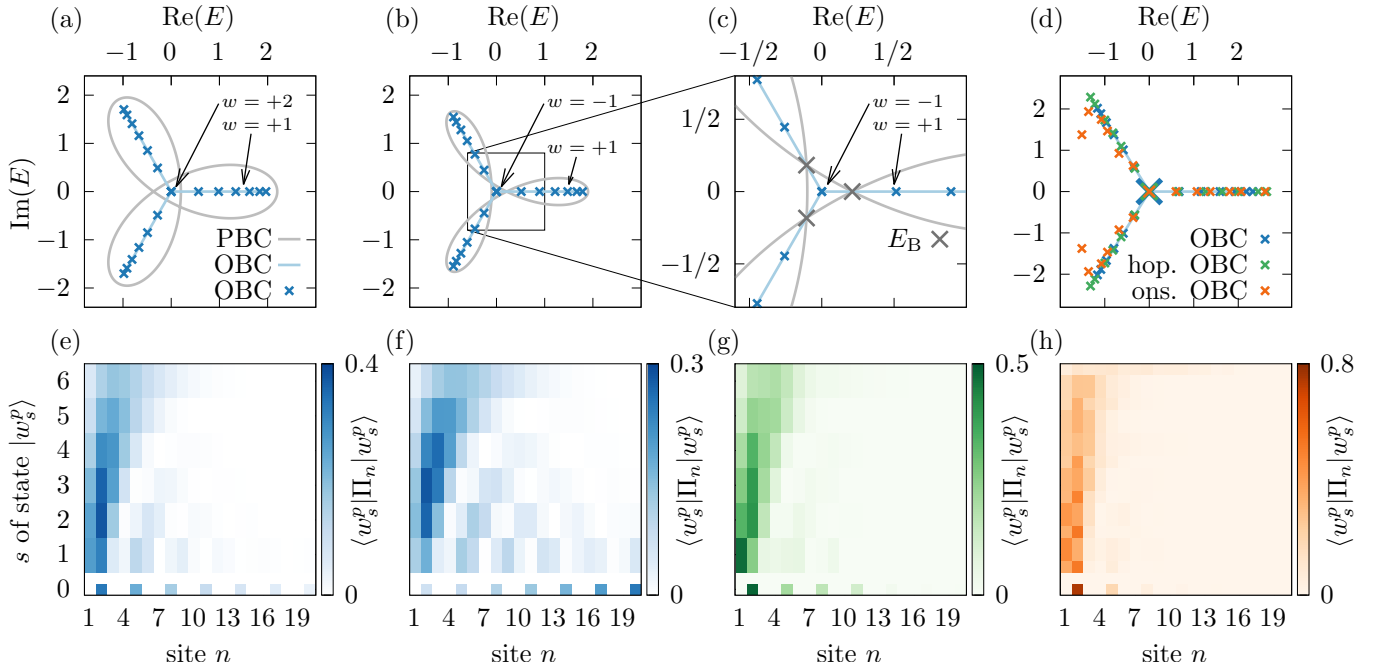


Figure 6. PBC (gray) and OBC (light blue) spectra and eigenstates of the generalized HN model with $l = 2$, $r = 1$ and $t_{-1} = 1$ for different hopping strengths t_2 and perturbations. OBC spectra for finite size (crosses) and associated eigenstates always correspond to a system of size $N = 20$ so that the system exhibits an EP2. All eigenstates are normalized so that $\langle w_s^p | w_s^p \rangle = 1$ where $\langle w_s^p | = (| w_s^p |)^\dagger$. (a) Spectra for $t_2 = 6/5 > t_{-1}$ showing only regions of positive winding number predicting that all eigenstates are localized on the left in (e). (b) Spectra for $t_2 = 9/10 < t_{-1}$ showing regions with winding numbers of opposite sign, thus predicting that all eigenstates associated with energies inside the $w = +1$ ($w = -1$) region are localized on the left (right). For $N = 20$, only the eigenstate associated with the EP is localized at the right, while all other eigenstates are localized at the left as shown in (f). (c) Zoom-in of (b) additionally marking the Bloch points (gray crosses). (d) Spectra for $t_2 = 2$ without perturbation (blue), with random perturbation in the hopping strengths characterized by $\Delta_l = \Delta_{-r} = 1/2$ (green) and random on-site disorder on SL_1 characterized by $W = 2$ (orange). In all cases, the EP2 at $E = 0$ stays unchanged. (e,f) Eigenvectors associated with (a,b). To depict the localization of the states, we plot $\langle w_s^p | \Pi_n | w_s^p \rangle$, where $\Pi_n = c_n^\dagger |0\rangle \langle 0| c_n$ is the projector onto each site in the chain. As such the phases p in Eq. (4) drop out and eigenvector are displayed in groups of three. (g,h) Eigenstates associated to the random perturbations in the hopping and random on-site disorder on SL_1 , respectively, with the spectrum in (d). One can clearly see that slight perturbations do not alter the NHSE.

Regarding the disorder in the hopping strengths, we remind ourselves that the generalized chiral symmetry only depends on the form Eq. (3), thus perturbing the hoppings $t_a \rightarrow t_{a,n}$, $a = l, -r$, does not break this symmetry. As such, the occurrence and order of the EPs only depends on the sizes of the SLs and is thus protected by the topology of the adjacency graph. If this topology is unaltered, i.e., $t_{a,n} \neq 0$ for all n , the EPs stay unaltered. For a change in the graph topology, i.e., setting some $t_{a,n} = 0$, the matter is more subtle. For example, splitting the system in smaller ones can leave the EP unchanged, e.g., removing all hoppings from and to the first red and yellow site in Fig. 3(a) splits the system of size N with $N \bmod 3 = 2$ into subsystems of size $N_1 = 3$ and $N_2 = N - 3$, where the former subsystem does not introduce new zero-energy solutions and the latter subsystem still exhibits an EP2. Another example would be to remove all the hoppings from a red site to green one via t_2 in Fig. 3(a). In any case, the occurrence of the NHSE crucially depends on the specific

values of the $t_{a,n}$. We find that introducing a random perturbation in the hoppings as $t_{a,n} = t_a(1 + \Delta_{a,n})$ with $\Delta_{a,n}$ uniform in $[-\Delta_a, +\Delta_a]$ does not destroy the NHSE for slight hopping disorders Δ_a , an insight carrying over from the customary HN model [40, 41]. A spectrum and its associated eigenvectors for a realization of such a random perturbation is shown in Figs. 6(d,g).

Let us now consider the second type of perturbation, on-site disorder. While the NHSE has been shown to be robust against on-site disorder up to a certain threshold as result of the spectral topology in case of the conventional HN model [12, 40, 41], EPs are not known to be stable against such perturbations. However, for the generalized HN model we showed that all generalized eigenvectors in a Jordan chain associated with a specific EP have weight only on specific SLs (in the example $l = 2$ and $r = 1$ on SL_2 and SL_3), but not on others (SL_1). Thus, any perturbation on the latter SLs will not affect the occurrence or order of that EP, even though it breaks the generalized chiral symmetry of \mathcal{H} . We show an ex-

ample for $l = 2$ and $r = 1$ with random on-site disorder on SL_1 modeled by $H_{\text{pert}} = \sum_n t_{0,n} \delta_{n \bmod 3,0} c_n^\dagger c_n$ where $t_{0,n}$ uniform in $[-W, +W]$ depicted in Figs. 6(d,h).

Not only is the EP robust against this form of perturbation, but one can also use on-site disorder as a mechanism to reduce the order of an EP by altering its Jordan chain. For example, for $l = 3$, $r = 1$ and $N \equiv -1 \bmod 4$ one has an EP3 with associated Jordan chain $H_{31}|\tilde{u}_0^4\rangle = |\tilde{u}_0^3\rangle$, $H_{31}|\tilde{u}_0^3\rangle = |\tilde{u}_0^2\rangle$ and $H_{31}|\tilde{u}_0^2\rangle = 0$. We introduce on-site disorder on SL_4 on which initially only $|\tilde{u}_0^4\rangle$ has weight, as $H_{\text{pert}} = \sum_n t_{0,n} \delta_{n \bmod 4,3} c_n^\dagger c_n$, with δ the Kronecker delta. We find that $|\tilde{u}_0^4\rangle$ is no longer a generalized eigenvector as $(H_{31} + H_{\text{pert}})|\tilde{u}_0^4\rangle = |\tilde{u}_0^3\rangle + H_{\text{pert}}|\tilde{u}_0^4\rangle \neq |\tilde{u}_0^3\rangle$. Introducing such an on-site term shifts one eigenvalue away from zero while keeping the remainder of the Jordan chain, thus reducing the EP3 to an EP2. Introducing on-site disorder on SLs associated with generalized eigenvectors within a Jordan chain, e.g., on SL_3 where $|\tilde{u}_0^3\rangle$ has weight, the matter is more subtle: One might falsely guess that this splits the EP3 into two one-dimensional zero-energy eigenspaces plus another non-zero subspace. However, in that example one can construct a new generalized eigenvector $|v\rangle$ with weight on SL_3 and SL_4 which satisfying $(H_{31} + H_{\text{pert}})|v\rangle = |\tilde{u}_0^2\rangle$, showing that the perturbed system still exhibits an EP2.

Discussion.—In this letter, we introduced the generalized HN model, where setting the hopping ranges l and r to the left and right, respectively, allows generating EPs of arbitrary order. In contrast to previously studied unidirectional models, the EPs we find do not scale with system size, while their existence does crucially depend on the system size. To the best of our knowledge, these type of system-size dependent EPs with system-size independent orders have not been systematically studied so far.

We find that the EPs in our system show remarkable features. Firstly, the eigenstates corresponding to the EPs are localized on a subset of sites we identified as SLs, independent of their hopping strengths. Tuning these hopping strengths, we are able to manipulate the NHSE so that the eigenstates associated with the EPs localize on a different end as compared to the remaining eigenstates of the system. Furthermore, as a result of the generalized chiral symmetry, the EPs are robust against generic perturbations in the hopping strength thus signalling that their occurrence finds its root in the spatial topology of the model. When we break the generalized chiral symmetry by introducing on-site disorder on specific SLs the EPs are either left unchanged or demoted in their order. We find that the NHSE does not vanish for any of the aforementioned perturbations for small perturbation strengths.

Other than the low-order EPs discussed in the main text, the generalized HN model exhibits another type of EP, which occurs when relaxing the constraint $t_l, t_{-r} > 0$ to also allow vanishing hopping strengths. Setting $t_{-r} =$

0 ($t_l = 0$) the generalized HN model decouples into l (r) unidirectional chains corresponding to EPs scaling with system size, which can be seen in Fig. 3(a) for $t_{-1} = 0$ ($t_2 = 0$).

We emphasize that the methods developed in this letter are applicable to any other model under OBCs, which can be brought into the form of Eq. (3). In this context, it is especially relevant to use the robustness against generic perturbations in the hopping strengths as well as the robustness against on-site disorder on specific SLs for the spectral features.

In this letter we inferred the spectrum and eigenvectors of \mathcal{H} from $\mathcal{H}^{l+r=n}$, which is the parent Hamiltonian in the context of n th-root topological phases [36, 42–46]. Deeper connections, such as how the spectral topology of both models is connected, fall outside the scope of this work, and remain an open question. Another fascinating direction is an analysis of our model in the context of topological graph theory. We find that the generalized HN model under OBCs (PBCs) can always be embedded onto a cylinder (torus). As such, our work is connected to so-called helical lattices [47–53].

Our generalized HN model can readily be implemented in experiment. There are several platforms, which allow for the implementation of unidirectional couplings, such as photonic ring systems [54], topoelectric circuits [1, 2], single-photon interferometry experiments simulating non-unitary quantum walks [55], and fiber loops modeling synthetic frequency dimensions [56, 57]. The realization of our model in the lab would allow for a rigorous study of the properties of EPs unaffected by perturbations.

ACKNOWLEDGMENTS

J.F. thanks Quentin Levoy for thoughtful discussions. J.T.G. and F.K.K. acknowledge funding from the Max Planck Society Lise Meitner Excellence Program 2.0. J.F. thanks the Max Planck School of Photonics for their generous support.

* julius.goehrlich@mpl.mpg.de

† flore.kunst@mpl.mpg.de

- [1] T. Helbig, T. Hofmann, S. Imhof, M. Abdelghany, T. Kiessling, L. W. Molenkamp, C. H. Lee, A. Szameit, M. Greiter, and R. Thomale, Generalized bulk-boundary correspondence in non-Hermitian topoelectrical circuits, *Nature Physics* **16**, 747 (2020).
- [2] T. Hofmann, T. Helbig, F. Schindler, N. Salgo, M. Brzezińska, M. Greiter, T. Kiessling, D. Wolf, A. Vollhardt, A. Kabaši, C. H. Lee, A. Bilušić, R. Thomale, and T. Neupert, Reciprocal skin effect and its realization in a topoelectrical circuit, *Physical Review Research* **2**, 023265 (2020).

[3] M.-A. Miri and A. Alù, Exceptional points in optics and photonics, *Science* **363**, eaar7709 (2019).

[4] H.-P. Breuer and F. Petruccione, *The Theory of Open Quantum Systems* (Oxford University Press, 2007).

[5] N. Moiseyev, Quantum theory of resonances: calculating energies, widths and cross-sections by complex scaling, *Physics Reports* **302**, 212 (1998).

[6] V. Kozii and L. Fu, Non-hermitian topological theory of finite-lifetime quasiparticles: Prediction of bulk fermi arc due to exceptional point, [arXiv:1708.05841](https://arxiv.org/abs/1708.05841).

[7] E. J. Bergholtz, J. C. Budich, and F. K. Kunst, Exceptional topology of non-Hermitian systems, *Reviews of Modern Physics* **93**, 015005 (2021).

[8] Y. Ashida, Z. Gong, and M. Ueda, Non-Hermitian physics, *Advances in Physics* **69**, 249 (2020).

[9] T. E. Lee, Anomalous Edge State in a Non-Hermitian Lattice, *Physical Review Letters* **116**, 133903 (2016).

[10] F. K. Kunst, E. Edvardsson, J. C. Budich, and E. J. Bergholtz, Biorthogonal Bulk-Boundary Correspondence in Non-Hermitian Systems, *Physical Review Letters* **121**, 026808 (2018).

[11] S. Yao and Z. Wang, Edge States and Topological Invariants of Non-Hermitian Systems, *Physical Review Letters* **121**, 086803 (2018).

[12] Z. Gong, Y. Ashida, K. Kawabata, K. Takasan, S. Higashikawa, and M. Ueda, Topological Phases of Non-Hermitian Systems, *Physical Review X* **8**, 031079 (2018).

[13] N. Okuma, K. Kawabata, K. Shiozaki, and M. Sato, Topological Origin of Non-Hermitian Skin Effects, *Physical Review Letters* **124**, 086801 (2020).

[14] K. Zhang, Z. Yang, and C. Fang, Correspondence between Winding Numbers and Skin Modes in Non-Hermitian Systems, *Physical Review Letters* **125**, 126402 (2020).

[15] F. K. Kunst and V. Dwivedi, Non-Hermitian systems and topology: A transfer-matrix perspective, *Physical Review B* **99**, 245116 (2019).

[16] W. D. Heiss, The physics of exceptional points, *Journal of Physics A: Mathematical and Theoretical* **45**, 444016 (2012).

[17] N. Hatano and D. R. Nelson, Localization Transitions in Non-Hermitian Quantum Mechanics, *Physical Review Letters* **77**, 570 (1996).

[18] N. Hatano and D. R. Nelson, Non-Hermitian delocalization and eigenfunctions, *Physical Review B* **58**, 8384 (1998).

[19] M. Berry, Physics of Nonhermitian Degeneracies, *Czechoslovak Journal of Physics* **54**, 1039 (2004).

[20] J. C. Budich, J. Carlström, F. K. Kunst, and E. J. Bergholtz, Symmetry-protected nodal phases in non-Hermitian systems, *Physical Review B* **99**, 041406 (2019).

[21] R. Okugawa and T. Yokoyama, Topological exceptional surfaces in non-Hermitian systems with parity-time and parity-particle-hole symmetries, *Physical Review B* **99**, 041202 (2019).

[22] P. Delplace, T. Yoshida, and Y. Hatsugai, Symmetry-Protected Multifold Exceptional Points and Their Topological Characterization, *Physical Review Letters* **127**, 186602 (2021).

[23] S. Sayyad and F. K. Kunst, Realizing exceptional points of any order in the presence of symmetry, *Physical Review Research* **4**, 023130 (2022).

[24] I. Mandal and E. J. Bergholtz, Symmetry and Higher-Order Exceptional Points, *Physical Review Letters* **127**, 186601 (2021).

[25] A. Montag and F. K. Kunst, Symmetry-induced higher-order exceptional points in two dimensions (), [arXiv:2401.10913](https://arxiv.org/abs/2401.10913).

[26] A. Montag and F. K. Kunst, Essential implications of similarities in non-hermitian systems (), [arXiv:2402.18249](https://arxiv.org/abs/2402.18249).

[27] Z.-J. Li, G. Cardoso, E. J. Bergholtz, and Q.-D. Jiang, Braids and higher-order exceptional points from the interplay between lossy defects and topological boundary states, [arXiv:2312.03054](https://arxiv.org/abs/2312.03054).

[28] P. Schmidt and F. Spitzer, The Toeplitz Matrices of an Arbitrary Laurent Polynomial, *Mathematica Scandinavica* **8**, 15 (1960).

[29] A. Böttcher and S. M. Grudsky, *Spectral Properties of Banded Toeplitz Matrices*, Other Titles in Applied Mathematics (Society for Industrial and Applied Mathematics, 2005).

[30] C. H. Lee, L. Li, R. Thomale, and J. Gong, Unraveling non-Hermitian pumping: Emergent spectral singularities and anomalous responses, *Physical Review B* **102**, 085151 (2020).

[31] T. Tai and C. H. Lee, Zoology of non-Hermitian spectra and their graph topology, *Physical Review B* **107**, L220301 (2023).

[32] F. Qin, R. Shen, L. Li, and C. H. Lee, Kinked linear response from non-hermitian pumping, [arXiv:2306.13139](https://arxiv.org/abs/2306.13139).

[33] S. M. Rafi-Ul-Islam, Z. B. Siu, H. Sahin, M. S. H. Razo, and M. B. A. Jalil, Twisted topology of non-Hermitian systems induced by long-range coupling, *Physical Review B* **109**, 045410 (2024).

[34] K. Yokomizo and S. Murakami, Non-Bloch Band Theory of Non-Hermitian Systems, *Physical Review Letters* **123**, 066404 (2019).

[35] Y. Xiong and H. Hu, Graph morphology of non-hermitian bands, *Phys. Rev. B* **109**, L100301 (2024).

[36] A. M. Marques and R. G. Dias, Generalized Lieb's theorem for noninteracting non-Hermitian \$n\$-partite tight-binding lattices, *Physical Review B* **106**, 205146 (2022).

[37] C. Yuce and H. Ramezani, Robust exceptional points in disordered systems, *EPL (Europhysics Letters)* **126**, 17002 (2019).

[38] J. D. H. Rivero and L. Ge, Origin of robust exceptional points: Restricted bulk zero mode, *Physical Review A* **101**, 063823 (2020).

[39] F. Song, S. Yao, and Z. Wang, Non-Hermitian Topological Invariants in Real Space, *Physical Review Letters* **123**, 246801 (2019).

[40] J. Claes and T. L. Hughes, Skin effect and winding number in disordered non-Hermitian systems, *Physical Review B* **103**, L140201 (2021).

[41] C. C. Wanjura, M. Brunelli, and A. Nunnenkamp, Correspondence between Non-Hermitian Topology and Directional Amplification in the Presence of Disorder, *Physical Review Letters* **127**, 213601 (2021).

[42] J. Arkinstall, M. H. Teimourpour, L. Feng, R. El-Ganainy, and H. Schomerus, Topological tight-binding models from nontrivial square roots, *Physical Review B* **95**, 165109 (2017).

[43] Z. Zhang, M. H. Teimourpour, J. Arkinstall, M. Pan, P. Miao, H. Schomerus, R. El-Ganainy, and L. Feng, Experimental Realization of Multiple Topological Edge States in a 1D Photonic Lattice, *Laser & Photonics Re-*

views **13**, 1800202 (2019).

[44] Z. Lin, S. Ke, S. Ke, X. Zhu, X. Zhu, and X. Li, Square-root non-Bloch topological insulators in non-Hermitian ring resonators, *Optics Express* **29**, 8462 (2021).

[45] L. Zhou, R. W. Bomantara, and S. Wu, $\$q\$$ th-root non-Hermitian Floquet topological insulators, *SciPost Physics* **13**, 015 (2022).

[46] W. Deng, T. Chen, and X. Zhang, $\$N\backslash\mathrm{th}\$$ power root topological phases in Hermitian and non-Hermitian systems, *Physical Review Research* **4**, 033109 (2022).

[47] O. V. Kibis, Electron-electron interaction in a spiral quantum wire, *Physics Letters A* **166**, 393 (1992).

[48] O. V. Kibis, S. V. Malevannyy, L. Huggett, D. G. W. Parfitt, and M. E. Portnoi, Superlattice Properties of Helical Nanostructures in a Transverse Electric Field, *Electromagnetics* **25**, 425 (2005).

[49] K. T. Law and D. E. Feldman, Quantum Phase Transition Between a Luttinger Liquid and a Gas of Cold Molecules, *Physical Review Letters* **101**, 096401 (2008).

[50] P. Schmelcher, Effective long-range interactions in confined curved dimensions, *Europhysics Letters* **95**, 50005 (2011).

[51] A. V. Zampetaki, J. Stockhöfe, S. Krönke, and P. Schmelcher, Classical scattering of charged particles confined on an inhomogeneous helix, *Physical Review E* **88**, 043202 (2013).

[52] J. K. Pedersen, D. V. Fedorov, A. S. Jensen, and N. T. Zinner, Formation of classical crystals of dipolar particles in a helical geometry, *Journal of Physics B: Atomic, Molecular and Optical Physics* **47**, 165103 (2014).

[53] A. V. Zampetaki, J. Stockhöfe, and P. Schmelcher, Degeneracy and inversion of band structure for Wigner crystals on a closed helix, *Physical Review A* **91**, 023409 (2015).

[54] D. Viedma, A. M. Marques, R. G. Dias, and V. Ahufinger, Topological n -root Su-Schrieffer-Heeger model in a non-Hermitian photonic ring system, *Nanophotonics* **13**, 51 (2024).

[55] K. Wang, L. Xiao, J. C. Budich, W. Yi, and P. Xue, Simulating Exceptional Non-Hermitian Metals with Single-Photon Interferometry, *Physical Review Letters* **127**, 026404 (2021).

[56] K. Wang, A. Dutt, K. Y. Yang, C. C. Wojcik, J. Vučković, and S. Fan, Generating arbitrary topological windings of a non-Hermitian band, *Science* **371**, 1240 (2021).

[57] A. Dutt, L. Yuan, K. Y. Yang, K. Wang, S. Buddhiraju, J. Vučković, and S. Fan, Creating boundaries along a synthetic frequency dimension, *Nature Communications* **13**, 3377 (2022).

Appendix A: The characteristic polynomial for $l = 2$ and $r = 1$

We proof the form of the characteristic polynomial of H_{21} of the main text, which we repeat here for convenience

$$\chi_N(E) = (-E)^d \sum_{m=0}^q \binom{N-2m}{m} (t_2 t_{-1}^2)^m (-E^3)^{q-m}, \quad (5)$$

where $N = 3q + d$ with $0 \leq d < 3$, where $q = \lfloor N/3 \rfloor$ is the quotient and $d = N \bmod 3$ is the remainder of the Euclidean division. We proof it in three steps: (i) writing down a linear recurrence equation, (ii) solving the linear recurrence relation in terms of generating functions, and (iii) rewriting this solution in the form presented in the main text.

To write down a linear recursion relation for the characteristic polynomial, we choose the N -dimensional matrix representation $\mathcal{H}_{N,21}^s$, where the label s signifies that we write it in the site basis,

$$\mathcal{H}_{N,21}^s = \begin{pmatrix} 0 & 0 & t_2 & & & & \\ t_{-1} & 0 & 0 & t_2 & & & \\ & t_{-1} & 0 & 0 & t_2 & & \\ & & \ddots & \ddots & \ddots & \ddots & \\ & & & t_{-1} & 0 & 0 & t_2 \\ & & & & t_{-1} & 0 & 0 \\ & & & & & t_{-1} & 0 \end{pmatrix}. \quad (6)$$

Then

$$\chi_N(E) = \det(\mathcal{H}_{N,21}^s - EI_N) = (-E) \det(\mathcal{H}_{N-1,21}^s - EI_{N-1}) + t_2 \det \begin{pmatrix} A & B \\ 0 & \mathcal{H}_{N-3,21}^s - EI_{N-3} \end{pmatrix}. \quad (7)$$

To find the equality, we use the Laplace expansion along the first row for the second equality, and

$$A = \begin{pmatrix} t_{-1} & -E \\ 0 & t_{-1} \end{pmatrix}, \quad B = \begin{pmatrix} t_2 & 0 & 0 & \cdots & 0 \\ 0 & t_2 & 0 & \cdots & 0 \end{pmatrix}. \quad (8)$$

Using a determinant identity for block matrices

$$\det \begin{pmatrix} A & B \\ 0 & D \end{pmatrix} = \det(A) \det(D) = \det \begin{pmatrix} A & 0 \\ C & D \end{pmatrix}, \quad (9)$$

where A , B , C and D are rectangular blocks, we can immediately determine the second determinant to find

$$\chi_N(E) = (-E)\chi_{N-1}(E) + t_2 t_{-1}^2 \chi_{N-3}(E). \quad (10)$$

As the recursion formula has an $N - 3$ dependence we need to determine three base cases. They are

$$\chi_1(E) = (-E)^1, \quad \chi_2(E) = (-E)^2, \quad \chi_3(E) = (-E)^3 + t_2 t_{-1}^2. \quad (11)$$

Even though it seems nonsensical to define the characteristic polynomial for $N = 0$, it will be useful to define $\chi_0(E) = (-E)^0 = 1$, which is consistent with the recursion relation and $\chi_3(E)$ from the previous equation, and use $\chi_0(E)$, $\chi_1(E)$ and $\chi_2(E)$ as base cases.

The next step is to find a generating function for $\chi_N(E)$ satisfying

$$S(x, E) = \sum_{N=0}^{\infty} \chi_N(E) x^N, \quad (12)$$

so that

$$\chi_N(E) = \frac{1}{N!} \left. \frac{d^N S(x, E)}{dx^N} \right|_{x=0}. \quad (13)$$

Multiplying the recurrence relation by x^N and summing over N we find an equation for $S(x, E)$,

$$\sum_{N=3}^{\infty} \chi_N x^N = \sum_{N=3}^{\infty} (-E \chi_{N-1} + T \chi_{N-3}) x^N, \quad (14)$$

where $T = t_2 t_{-1}^2$ and we start the sum at $N = 3$ for reasons that become apparent below, and we drop the E dependence of χ for readability. After some index shifts, we have

$$\sum_{N=3}^{\infty} \chi_N x^N = -Ex \sum_{N=2}^{\infty} \chi_N x^N + Tx^3 \sum_{N=0}^{\infty} \chi_N x^N. \quad (15)$$

To get back $S(x, E)$, we subtract and add the appropriate terms as

$$\sum_{N=0}^{\infty} \chi_N x^N = \sum_{N=0}^{m-1} \chi_N x^N + \sum_{N=m}^{\infty} \chi_N x^N \quad (16)$$

to find

$$S(x, E) - \sum_{N=0}^2 \chi_N x^N = -Ex \left[S(x, E) - \sum_{N=0}^1 \chi_N x^N \right] + Tx^3 S(x, E). \quad (17)$$

Using the base cases $\chi_n = (-E)^n$ for $n = 0, 1, 2$ and rearranging we find the generating function

$$S(x, E) = \frac{1}{1 + Ex - Tx^3}. \quad (18)$$

Finally, we want to prove that the generating function $S(x, E)$ generates Eq. (5), which we repeat in a slightly different form here

$$\chi_N(E) = \sum_{m=0}^{\lfloor N/3 \rfloor} \binom{N-2m}{m} (t_2 t_{-1}^2)^m (-E)^{N-3m}. \quad (19)$$

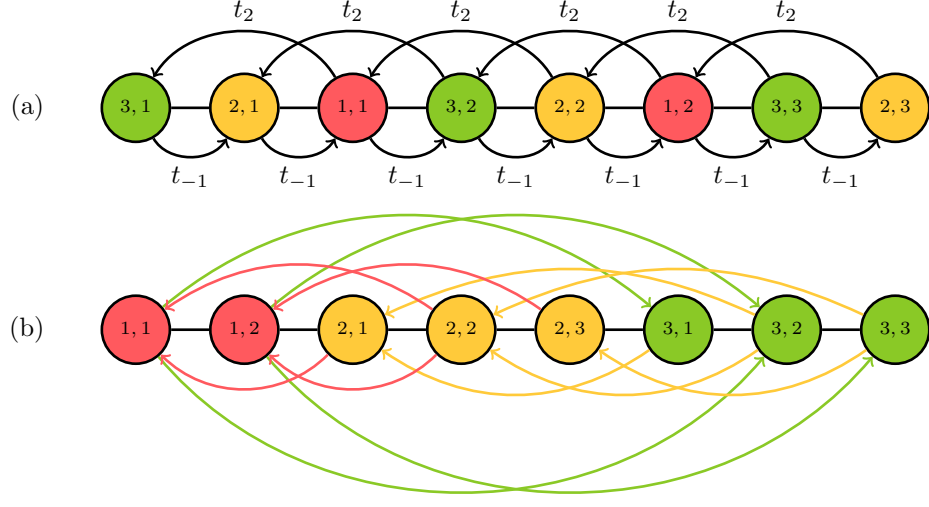


Figure 7. Generalized HN model for $l = 2$, $r = 1$ and $N = 8$. Each node contains j, i , where j refers to SL_j and i to the index within each SL. (a) Model in site basis. (b) Model in the transformed basis. Red, yellow and green arrows correspond to entries in h_1 , h_2 and h_3 , respectively. Hoppings above (below) the chain corresponds to t_2 (t_{-1}).

Setting $N = 3q + d$ via Euclidean division proofs Eq. (5). We can expand the generating function using the geometric series as

$$S(x, E) = \frac{1}{1 - (-Ex + Tx^3)} = \sum_{n=0}^{\infty} (-Ex + Tx^3)^n = \sum_{N=0}^{\infty} \chi_N(E) x^N \quad (20)$$

To determine the characteristic polynomial we need to match terms. We start by considering the coefficient of E^k multiplying x^N , i.e., the coefficient of E^k in $\chi_N(E)$. First off, notice that unless $k \equiv N \pmod{3}$, the coefficient will be 0. This is because all the terms will be products of $-Ex$ and Tx^3 , and multiplying an expression by $-Ex$ increases the exponent of both E and x by 1, while multiplying by Tx^3 raises the exponent of x by 3. Next, note that the coefficient of E^N multiplying x^N is simply $(-1)^N$, since the only product which achieves an $E^N x^N$ term is $(-Ex)^N$. The coefficient of E^{N-3} is $T(-1)^{N-1}(N-2)$. This is because $E^{N-3} x^N$ is achieved by multiplying $(N-3)$ terms of $-Ex$ with 1 term of Tx^3 . There are $(N-2)$ terms in total, so there are $\binom{N-2}{N-3} = N-2$ ways to order them. The term with exponent $E^{N-3m} x^N$ is achieved by multiplying $(N-3m)$ terms of $-Ex$ with m terms of Tx^3 . There are $(N-2m)$ terms in total, and therefore $\binom{N-2m}{m}$ different ways to form a product with exponent $E^{N-3m} x^N$. The coefficient is therefore $T^m (-1)^{N-3m} \binom{N-2m}{m}$, concluding the proof.

A similar analysis could find expressions for any rational function in terms of binomial coefficients.

Appendix B: Properties of h_j

In order to state some general properties of the h_j we start again by considering the generalized HN model. Let us start by considering it in the site basis so that its matrix elements are given by $(\mathcal{H}_{lr}^s)_{m,n} = t_l \delta_{m,n-l} + t_{-r} \delta_{m,n+r}$. \mathcal{H}_{lr}^s is similar to \mathcal{H}_{lr} using a permutation matrix. Without loss of generality, we choose the permutation matrix, which keeps the order within each SL unchanged, i.e., the i th site on SL_j in the site basis gets mapped to the i th site on SL_j in the transformed basis. Over all, one can convince oneself that that one can either hop from SL index i to i and from $i+1$ to i , or one can hop from i to i and i to $i+1$, cf. Fig. 7(b). By carefully considering the individual SL sizes and hopping strengths, one can find that the matrix elements of h_j are either $(h_j)_{m,n} = t_{-r} \delta_{m,n} + t_l \delta_{m,n-1}$ or $(h_j)_{m,n} = t_{-r} \delta_{m,n+1} + t_l \delta_{m,n}$. An example for $l = 2$, $r = 1$ and $N = 8$ is shown in Fig. 7.

In the main text we use that the h_j of size $d_j \times d_j$ have trivial nullspace, i.e., there exists no $|v\rangle \neq 0$ so that $h_j |v\rangle = 0$. From the explicit form of h_j in that case it is clear that it has full rank as $t_l, t_{-r} \neq 0$. Thus, by the rank-nullity theorem we have $\text{rank}(h_j) + \text{nullity}(h_j) = d_j$, and we find h_j has trivial nullspace.